Weierstraß-Institut
für Angewandte Analysis und Stochastik
Leibniz-Institut im Forschungsverbund Berlin e. V.

Preprint ISSN 2198-5855

Emergence and combinatorial accumulation of jittering regimes in spiking oscillators with delayed feedback

Vladimir Klinshov[1,2], Leonhard Lücken[3], Dmitry Shchapin[1,2],

Vladimir Nekorkin[1,2], Serhiy Yanchuk[3]

submitted: June 10, 2015

[1] Institute of Applied Physics of the Russian Academy of Sciences
46 Ul'yanov Street
603950, Nizhny Novgorod
Russia
E-Mail: vladimir.klinshov@gmail.com

[2] University of Nizhny Novgorod
23 Prospekt Gagarina
603950, Nizhny Novgorod
Russia

[3] Weierstrass Institute
Mohrenstr. 39
10117 Berlin
Germany
E-Mail: leonhard.luecken@wias-berlin.de
serhiy.yanchuk@wias-berlin.de

No. 2126

Berlin 2015

2010 *Mathematics Subject Classification.* 37G15, 37N20, 92B25.

2008 *Physics and Astronomy Classification Scheme.* 87.19.ll, 05.45.Xt, 87.19.lr, 89.75.Kd.

Key words and phrases. Phase oscillator, delayed feedback, pulsatile feedback, jitter, degenerate bifurcation, PRC.

The theoretical study was supported by the Russian Foundation for Basic Research (Grants No. 14-02-00042 and No. 14-02-31873), the German Research Foundation (DFG) in the framework of the Collaborative Research Center SFB 910, Erasmus Mundus Aurora consortium (grant number AURORA2012B1246), and the European Research Council (ERC-2010-AdG 267802, Analysis of Multiscale Systems Driven by Functionals). The experimental study was carried out with the financial support of the Russian Science Foundation (Project No. 14-12-01358).

Edited by
Weierstraß-Institut für Angewandte Analysis und Stochastik (WIAS)
Leibniz-Institut im Forschungsverbund Berlin e. V.
Mohrenstraße 39
10117 Berlin
Germany

Fax: +49 30 20372-303
E-Mail: preprint@wias-berlin.de
World Wide Web: http://www.wias-berlin.de/

Abstract

Interaction via pulses is common in many natural systems, especially neuronal. In this article we study one of the simplest possible systems with pulse interaction: a phase oscillator with delayed pulsatile feedback. When the oscillator reaches a specific state, it emits a pulse, which returns after propagating through a delay line. The impact of an incoming pulse is described by the oscillator's phase reset curve (PRC). In such a system we discover an unexpected phenomenon: for a sufficiently steep slope of the PRC, a periodic regular spiking solution bifurcates with several multipliers crossing the unit circle at the same parameter value. The number of such critical multipliers increases linearly with the delay and thus may be arbitrary large. This bifurcation is accompanied by the emergence of numerous "jittering" regimes with non-equal interspike intervals (ISIs). The number of the emergent solutions increases exponentially with the delay. We describe the combinatorial mechanism that underlies the emergence of such a variety of solutions. In particular, we show how each periodic solution consisting of different ISIs implies the appearance of multiple other solutions obtained by rearranging of these ISIs. We show that the theoretical results for phase oscillators accurately predict the behavior of an experimentally implemented electronic oscillator with pulsatile feedback.

1 Introduction

Oscillating systems subject to pulsed inputs or interactions were studied in many different areas, such as dynamics of spiking neurons [1], communication of fireflies by short light pulses [2, 3], impacting mechanical oscillators [4], electronic oscillators [5–7], optical systems [8–10], stimulation of cardiac [11–13], respiratory [14, 15] or circadian [16] rhythms. Simple but powerful models to describe such systems are phase oscillators with pulsatile coupling, which are especially popular in neuroscience [2, 17–31]. Apart of the simplicity of phase models in comparison to conductance-based models [33], they possess two main features: the possibility of individual neurons to produce periodic output, and the fact that interaction between neurons is mediated by the brief action potentials or spikes, which have a temporal duration much smaller than the interspike intervals (ISIs). Moreover, the effect of a spike depends on the dynamical state at which the neuron is located at the time of the spike arrival. In phase models such an effect is incorporated with the help of phase reset curves (PRC) [3, 28, 34–36]. In its representation as a phase oscillator, each type of neuron possesses a characteristic PRC corresponding to a particular stimulus. Hence, parameter changes in the neuron or the stimulus are reflected by changes in the shape of the PRC. PRCs can be computed for any oscillatory system and stimulus including neuronal models such as Hodgkin-Huxley, FitzHugh-Nagumo, and others [35, 37]. In this way, pulse-coupled systems can be considered either as stand-alone models, or as approximations of coupled oscillatory conductance-based systems. Among the advantages

of such models is their simple numerical implementation, their lower dimension in comparison with conductance-based models, as well as the possibility to adjust the PRC numerically and measure it experimentally [38–41] in order to find characteristics of the individual neurons. The phase description can serve as an appropriate approximation, if the responses of the system to inputs introduce transient deviations from the oscillatory state, which are shorter than the ISIs.

In this paper we consider a single oscillator with pulsatile delayed feedback extending the results reported in [32]. The study on this basic "motif" is important for understanding the behavior of larger delay-coupled networks [42]. For instance, a loop consisting of one excitatory and one inhibitory neuron with delayed connection shows similar behavior to a neuron with delayed self-feedback [43–45], and also the behavior of rings of several neurons are, in some cases, related to the behavior of a single neuron with delayed feedback [46–48]. In fact, a larger neuronal feedback delay might firstly arise due to a chained propagation of action potentials along a ring of neurons. Another motivation to study a single oscillator with delayed feedback arises from the study of ensembles of delay coupled oscillators where the synchronous regime and some modes of its instability can be described by the behavior of a single oscillator [49].

Although we approach the problem of an oscillator with pulsed feedback from a general perspective, not bound to a specific area of application, neurons with delayed feedback are a prototypical example for such systems. There exist some studies on this subject [43–45, 50, 51], all of which have a common baseline: delay leads to immense multistability. At first glance this result is not too surprising since multistability generically arises in delay differential equations due to a well-known mechanism called "periodic solution reappearance" [52]. Interestingly, in the case of a pulsatile feedback, this mechanism does not always explain the large variety of observed solutions. Another property, which is connected to some combinatorial relations between the ISIs is responsible for the extreme multistability which arises for larger values of the feedback delay. For example, Ma and Wu [43, 44] found for several neuron models that a large number of periodic solutions coexists. Remarkably, these solutions exhibit only a few distinct ISIs; moreover, different solutions can be transformed into another by permuting the order of the ISIs. Our results shed some light on these earlier works from another perspective.

We show that an oscillatory system with delayed pulsatile feedback may generically exhibit a very surprising phenomenon, which manifests itself as follows: under some conditions a periodical regime of regular spiking destabilizes in a degenerate manner such that several multipliers (Lyapunov exponents) become critical at once. The number of the critical multipliers is proportional to the feedback delay and can be arbitrary large. Thus, the dimension of the unstable manifold of the regular spiking solution changes abruptly from zero to an arbitrary large value, which we call the "dimension explosion" phenomenon. As a result of such a bifurcation, we show that there appear multiple coexistent "jittering" solutions, characterized by non-equal ISIs. This leads us to call the bifurcation a "multi-jitter" bifurcation. We prove that the number of the emergent jittering solutions grows exponentially with the delay.

The structure of the paper is as follows: In section 2 we introduce the model for a phase oscillator with delayed pulsatile feedback, introduce some definitions and assumptions, and give the system's reformulation as discrete return map of ISI-sequences. In section 3 we study the regime of regular spiking (RS) where all ISIs are identical. We obtain an explicit parametric expression for all branches of RS solutions, determine their stability, and give conditions for the

multi-jitter bifurcation. It turns out that the crucial quantity involved is the steepness of the PRC. In the following Section 4 we undertake a numerical exploration of the system's behavior beyond the multi-jitter bifurcation and report a huge multistability of periodic solutions and chaotic attractors. The most dominant type of the observed solutions exhibits a periodic repetition of only two different ISIs in seemingly arbitrary order. We explain this phenomenon in section 5 where we prove that the phenomenon of dimension explosion is indeed accompanied by an explosion of the number of coexisting solutions. In Section 6 we present an experimental realization, where the effects predicted by the phase model can be observed in an electronic oscillator. We conclude with a discussion in section 7.

2 Model

We consider an oscillator with delayed pulsatile feedback of the form [24, 27, 28, 30–32, 53]:

$$\frac{d\varphi}{dt} = 1 + Z(\varphi) \sum_{t_j} \delta(t - t_j - \tau). \tag{1}$$

The oscillator is described by its phase φ, which changes on the circle $[0, 1]$ with $\varphi = 0$ and $\varphi = 1$ identified. In the case without delayed feedback, the phase grows uniformly with normalized frequency $\omega = 1$. When the phase reaches unity, the oscillator is assumed to emit a pulse. The instants when the pulses are emitted are denoted by t_j, $j = 1, 2, \ldots$. The emitted pulses propagate along the feedback line and affect the oscillator after the delay τ at the time instants $t_j^* = t_j + \tau$. When a pulse is received, the phase of the oscillator undergoes an instantaneous, discontinuous shift, and changes its value to the new value

$$\varphi(t_j^* + 0) = \varphi + Z(\varphi),$$

where $\varphi = \varphi(t_j^* - 0)$ and the function $Z(\varphi)$ is the PRC. In the following, we suppose that $Z(\varphi)$ is continuous and differentiable for all φ. Further, we assume that

$$Z(0) = Z(1) = 0, \tag{2}$$

which means that the oscillator does not respond to perturbations during its own spike. In some cases, such an assumption is reasonable, especially for the modeling of neuronal dynamics involving a fast change in the systems state around $\varphi = 0$, see additional discussion in [30, 31]. We also impose that

$$\varphi + Z(\varphi) \in [0, 1] \tag{3}$$

for all $\varphi \in [0, 1]$.

For numerical illustrations we consider the PRC

$$Z(\varphi) = \kappa \times (\sin(\pi\varphi))^q, \tag{4}$$

which is shown in Fig. 1. Here $\kappa > 0$ is the feedback strength, and $q > 1$ is a parameter that controls the steepness of the PRC, which is the crucial quantity for the dynamical phenomena reported in this paper. We define the steepness as the maximal *downward* slope of Z:

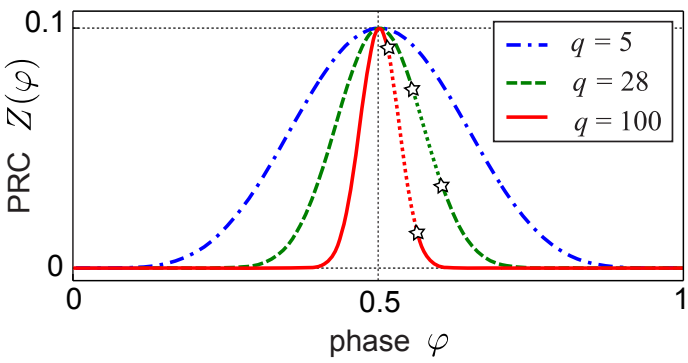

Figure 1: PRC function (4) for different values of the parameter q. Stars indicate points, where $Z'(\varphi) = -1$ corresponding to possible multi-jitter bifurcations [see Sec. 3.2].

$$s := \left| \inf_{\varphi \in (0,1)} Z'(\varphi) \right|. \tag{5}$$

We emphasize, that the particular shape and amplitude of the PRC is not important for our results and the reported phenomena can be observed for any PRC satisfying conditions (2)–(3), and possessing a sufficiently high steepness. For the function (4) the steepness can be estimated for large q as

$$s \approx \kappa \times \pi \sqrt{q/e}, \tag{6}$$

where e is Euler's number [see Appendix A].

As for any system with time delay, some amount of information about its past is required for system (1) in order to determine its future evolution. However, because of the pulsatile nature of the feedback, the only information needed is the time-moments of the pulses t_j. In [54] it was proven that a system with pulsatile delayed coupling can be reduced to a finite-dimensional map under quite general conditions. For the oscillator (1) such a map can be obtained for the ISIs $T_j = t_j - t_{j-1}$:

$$T_{j+1} = F\left(T_j, T_{j-1}, ..., T_{j-P+1}\right). \tag{7}$$

The map (7) determines the next ISI based on the P preceding ISIs. Equation (7) can equivalently be written as the P-dimensional map

$$(T_1, ..., T_P) \mapsto (T_2, ..., T_P, F(T_1, ..., T_P)).$$

According to [54], the map dimension is bounded as follows:

$$P \leq 1 + \frac{\tau}{1 - 2Z_{\max}},$$

where $Z_{\max} = \max_{0 \leq \varphi \leq 1}(Z(\varphi))$. For the PRC (4), $Z_{\max} = \kappa$.

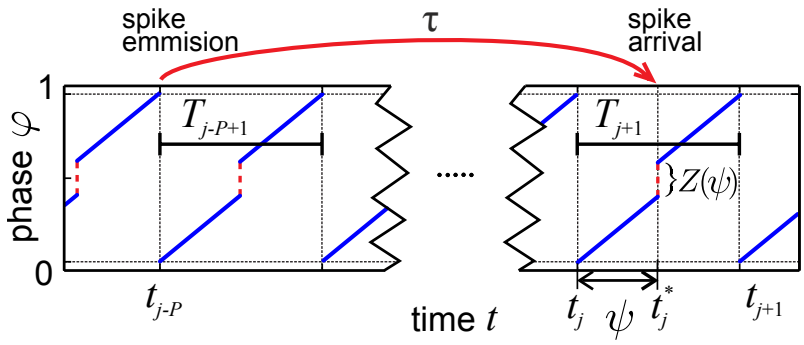

Figure 2: Spiking dynamics schematically. The spike emitted at t_{j-P} affects the dynamics after time delay τ at $t_j^* = t_{j-P} + \tau$.

3 Regular spiking

The map (7) can have different and complicated forms depending on the relation between the delay time and the spiking frequency [54]. Therefore, we will not write down the general form of F here. Instead, we derive the form of the map for the case when there is only one feedback spike arriving at the oscillator during each ISI. In particular, this form is always adequate in the case when the oscillator is in a RS regime. Each RS regime corresponds to a fixed point of (7), and is characterized by a repeated spiking with a constant ISI length $T_j \equiv T$ for all j.

Under the assumption that exactly one spike arrives per ISI, let us consider the oscillator dynamics on the time interval $[t_j, t_{j+1}]$. First, note that there exists a unique number P of ISIs between t_j and the emission time t_{j-P} of the spike arriving at $t_j^* \in [t_j, t_{j+1}]$, cf. Fig. 2. Accordingly, we have

$$t_j^* = t_{j-P} + \tau = t_j + \tau - \sum_{k=j-P+1}^{j} T_k.$$

Further, the oscillator's phase φ grows from zero to one within the interval $[t_j, t_{j+1}]$, and, except from the instant t_j^* when a feedback pulse arrives and perturbs the phase, it grows linearly with time. The phase value $\psi \in [0, 1]$ at the moment of the pulse arrival equals

$$\psi = t_j^* - t_j = \tau - \sum_{k=j-P+1}^{j} T_k. \tag{8}$$

Hence the corresponding shift of the perturbed phase equals $Z(\psi)$ and the oscillator's phase immediately after the pulse impact is $\varphi(t_j^* + 0) = \psi + Z(\psi)$. Finally, the ISI

$$T_{j+1} = t_{j+1} - t_j = \psi + t_{j+1} - t_j^*$$

is determined from the condition $\varphi(t_{j+1}) = 1$:

$$\begin{aligned} 1 = \varphi(t_{j+1}) &= \psi + Z(\psi) + t_{j+1} - t_j^* \\ &= T_{j+1} + Z\left(\tau - \sum_{k=j-P+1}^{j} T_k\right). \end{aligned}$$

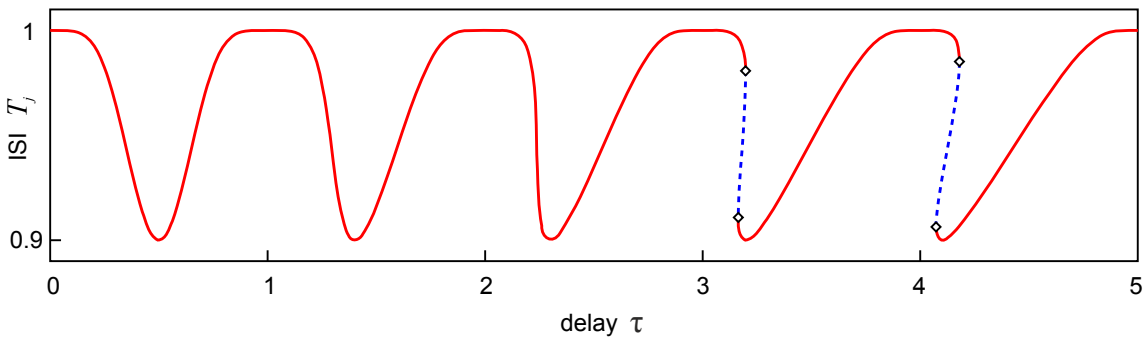

Figure 3: One-dimensional bifurcation diagram for the ISIs T of RS solutions versus delay τ according to (11) with $Z(\varphi)$ from Eq. (4) and $q = 5$. Red solid lines correspond to stable RS, blue dashed lines correspond to unstable RS [cf. Sec. 3.2]. The squares indicate fold bifurcations.

Hence, for (7) we obtain the form

$$T_{j+1} = 1 - Z\left(\tau - \sum_{k=j-P+1}^{j} T_k\right). \tag{9}$$

3.1 Existence of RS

In the case of RS the oscillator emits pulses periodically with $t_j = jT$ and $T_j = T$ for all j. This implies, that there is exactly one spike within each interval $[t_j, t_{j+1})$ and the ISI map necessarily takes the form (9). RS solutions correspond to fixed points of (9) and therefore all possible periods T are given as solutions to

$$T = 1 - Z\left(\tau - PT\right) \tag{10}$$

where $P = [\tau/T]$ is the number of full periods within one delay interval ($[\cdot]$ denotes the integer part). Thus, $\tau = PT + \psi$ with $\psi := \tau \mod T$, and we can write Eq. (10) in the parametric form:

$$\begin{aligned} T &= 1 - Z(\psi), \\ \tau &= P\left(1 - Z(\psi)\right) + \psi. \end{aligned} \tag{11}$$

The advantage of Eq. (11) as compared to Eq. (10) is that it allows an explicit representation of all RS solutions (i.e. their periods T) as a function of τ. The curve $(\tau(\psi), T(\psi))$ obtained by substituting $P = 0, 1, 2, \ldots$ in (11) and varying ψ within the interval $[0, 1]$ is shown in Fig. 3. An important consequence of this dependency is that for each value of τ at least one value of T exists. For small values of τ the expression $T(\tau)$ is single-valued, but for larger τ folding takes place leading to an emergence of several solution branches. The fold points satisfy

$$0 = \frac{\partial \tau}{\partial T} = \frac{\partial \tau}{\partial \psi}\left(\frac{\partial T}{\partial \psi}\right)^{-1} = \frac{1 - PZ'(\psi)}{-Z'(\psi)},$$

that is,

$$PZ'(\psi) \;=\; 1. \tag{12}$$

From Eq. (12) it is clear that folds do not occur for $P < 1/|\max_{0\leq\varphi\leq 1} Z'(\varphi)|$. For larger P intervals of τ appear for which several different RS solutions with different periods coexist. As follows from a general result derived in [52], the number of coexisting RS solutions grows linearly with the time-delay τ.

3.2 Linear stability

Let us analyze the linear stability of the RS solutions. For this we introduce small perturbations δ_j to the initial conditions such that $T_j = T + \delta_j$, and study whether the perturbations are damped or amplified with time. Since small perturbations do not violate the property that only one spike occurs within each interval $[t_j, t_{j+1}]$, the map (9) can be used to study their evolution relevant to the stability of the corresponding RS solution. We substitute $T_j = T + \delta_j$ into (9), linearize the obtained expression with respect to δ_j, and obtain the map

$$\delta_{j+1} = Z'(\psi) \sum_{k=j-P+1}^{j} \delta_k, \tag{13}$$

where $\psi = \tau - PT$. The stability of the linear map (13) is described by its characteristic multipliers $\lambda \in \mathbb{C}$, that is, by the roots of the characteristic equation

$$\chi_{P,\alpha}(\lambda) = \lambda^P - \alpha \sum_{k=0}^{P-1} \lambda^k = 0 \tag{14}$$

where $\alpha := Z'(\psi)$. If Eq. (14) has only multipliers with $|\lambda| < 1$ the corresponding RS regime is locally stable. The following statements summarize properties of the multipliers [see Appendix B for details]:

(A) For $-1 < \alpha < 1/P$, all multipliers have absolute values less than one. As a result, the RS solution is asymptotically stable.

(B) At $\alpha = 1/P$ one critical multiplier crosses the unit circle at $\lambda = 1$. For $\alpha > 1/P$ this multiplier remains unstable.

(C) At $\alpha = -1$ there are P critical multipliers $\lambda_k = e^{i2\pi k/(P+1)}$, $k = 1, \ldots, P$, crossing $|\lambda| = 1$ simultaneously. For $\alpha < -1$, there are P unstable multipliers with $|\lambda_k| > 1$, $k = 1, \ldots, P$.

Figure 4 illustrates the possible spectra for different values of the parameter α. The stability region for regular spiking is $-1 < \alpha < 1/P$. For $\alpha = 1/P$ the stability is lost through a saddle-node bifurcation corresponding to the fold described by (12).

The most remarkable destabilization scenario is related to the transition at the parameter value $\alpha = -1$, where P multipliers become unstable simultaneously if α is decreased. At this point the dimension of the unstable manifold increases abruptly from 0 (stable RS solution) to P, which can be arbitrary large depending on the size of the delay τ. Although this "dimension explosion" seems to be very degenerate, it occurs generically within our setup. In the following we study this surprising bifurcation.

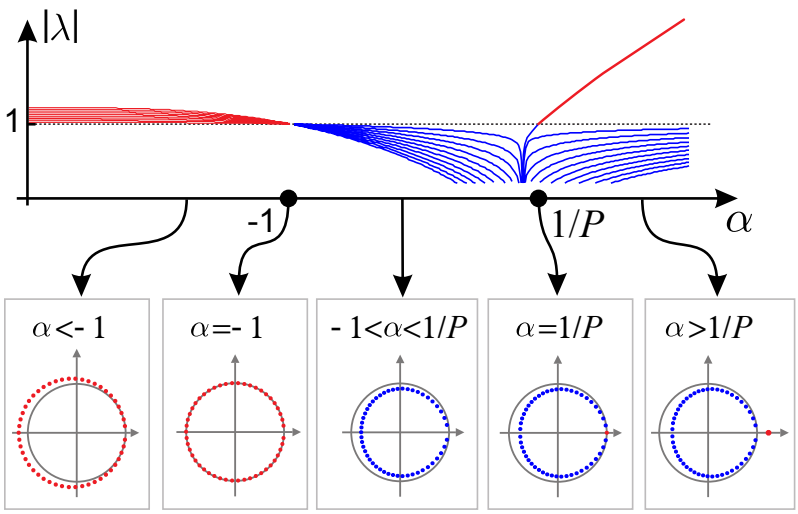

Figure 4: Multipliers λ of the RS solution versus the parameter α. Blue lines depict the stable part of the spectrum, red the unstable part.

4 Numerical study of jittering

In this section we show numerically, that a destabilization of RS taking place at $\alpha = -1$ leads to the emergence of a variety of "jittering" spiking modes with non-identical ISIs T_j. In order to achieve the bifurcation condition $\alpha = Z'(\psi) = -1$, the steepness s of the PRC should satisfy $s \geq 1$. For the PRC given by Eq. (4), the steepness is given by (6), and the condition $s \geq 1$ leads to $q \geq q^*$ with $q^* \approx e/(0.1\pi)^2 \approx 27.5$.

To explore the regimes of irregular spiking we first study the map (9) for the PRC (4) with $\kappa = 0.1$. A series of bifurcation diagrams is shown in Figs. 3, 5, and, 6. They illustrate the observed ISIs of the system for continuously varying delay τ and three different values, $q = 5, 28$, and 100, of the steepness parameter. For each value of the delay τ we simulated the system 20 times starting from random initial conditions (initial ISIs were drawn from a uniform distribution in $[0.9, 1.0]$). For each simulation all different values of ISIs T_j, which could be observed after a transient, were saved. For each observed value T_j a red dot was placed at coordinate (τ, T_j). Further, the parametric representation (11) was utilized to draw a line corresponding to RS solutions. It is solid red where the RS is stable and dashed blue where it is unstable, as determined from the condition $\alpha \in (-1, 1/P)$.

4.1 Subcritical steepness

Figure 3 shows the case $q = 5 < q^*$, where the only possible bifurcations are folds of the RS. This means, for each value of τ, each single point (τ, T) on the bifurcation diagram corresponds to one possible RS solution. Intervals of τ where two distinct values of T appear correspond to different coexisting RS solutions with distinct periods. The periods of the observed regular spiking are determined analytically by (11).

When the steepness of the PRC increases and q exceeds the critical value q^*, two points

$\psi_{A,B} \in (0,1)$ appear for which $Z'(\psi_{A,B}) = -1$. This means that for appropriate values of the delay time τ, such that $\psi = \tau \bmod T$ equals either to ψ_A or ψ_B, the stability of the RS changes and P multipliers cross the unit circle simultaneously, where $P = [\tau/T]$. More precisely: for each $P \in \mathbb{N}$, there exist two values of the delay [cf. (11)],

$$\tau_{A,B}^P = P(1 - Z(\psi_{A,B})) + \psi_{A,B}, \tag{15}$$

for which the dimension of the unstable manifold of the RS explodes from 0 to P.

4.2 Moderate supercritical steepness

Figure 5 illustrates the case close to criticality with $q = 28$, corresponding to $s \approx 1.017$, and slightly larger than the critical parameter value $q^* \approx 27.5$. The newly occurring bifurcations are located on the stable, upward part of the RS branch and the panels 5(b-d) show enlarged neighborhoods of the corresponding intervals $[\tau_A^P, \tau_B^P]$ for $P = 1, 3, 4$.

As shown in Section 3.2, P multipliers $\lambda_k = e^{i2\pi k/(P+1)}$ cross the unit circle simultaneously at $\tau = \tau_{A,B}^P$. For the case $P = 1$, this means only one multiplier $\lambda = -1$ crosses the unit circle in the points $\tau = \tau_{A,B}^1$. Note that in this case the map (9) is one-dimensional and has the form

$$T_{j+1} = 1 - Z\left(\tau - T_j\right). \tag{16}$$

In this case, the bifurcation is a supercritical period doubling giving birth to a stable period-2 solution existing for τ in the interval $[\tau_A^1, \tau_B^1]$. For this solution the spiking regime is "jittering": the ISIs T_j are not equal anymore but they form an alternating sequence with $T_{2j+1} = T_1$ and $T_{2j} = T_2$, with $T_1 \neq T_2$. The temporal dynamics of the ISIs for the period-2 solution is illustrated in Fig.5(e) together with a corresponding cobweb-diagram for the one-dimensional map (16). In the bifurcation diagram Fig. 5(a) a period-2 solution corresponds to a pair of points (τ, T_1) and (τ, T_2).

For $P \geq 2$ bifurcations take place, where P multipliers simultaneously becoming unstable at $\tau = \tau_{A,B}^P$. The RS solution loses its stability inside the interval $\tau \in \left[\tau_A^P, \tau_B^P\right]$, and various stable "jittering" regimes with non-equal ISIs appear. In numerical studies we observe that the emerging solutions have period $(P+1)$. However, a consistent property of these period-$(P+1)$ solutions is that their ISIs consist of only two (or less often three) different values of T_j. An example of such a period-4 solution at $P = 3$ is given in Fig. 5(f), where the corresponding ISI sequence has the form $(\overline{T_1, T_1, T_2, T_2}) := (\ldots, T_1, T_1, T_2, T_2, \ldots)$. Here and in the following, the periodically repeating part of the solution is denoted with an overline. As a result, such solutions correspond to only two, and not $P + 1$ points on the bifurcation diagram in Fig. 5(a). Since this type of solutions appear to be prevalent in the considered system, we will introduce the term *bipartite* solutions to refer to them. Analogously, we use the term *tripartite* solutions for solutions exhibiting three different ISIs.

For each $P \geq 2$, a variety of different bi- or tripartite solutions with period $P + 1$ is observed inside the interval $\tau \in \left[\tau_A^P; \tau_B^P\right]$. Moreover, some of them exist in a wider parameter interval. We denote this interval as $\left[\tau_C^P; \tau_D^P\right]$. The stability regions of different bipartite solutions alternate inside this interval, so that different solutions are observed as the delay is changed. For example,

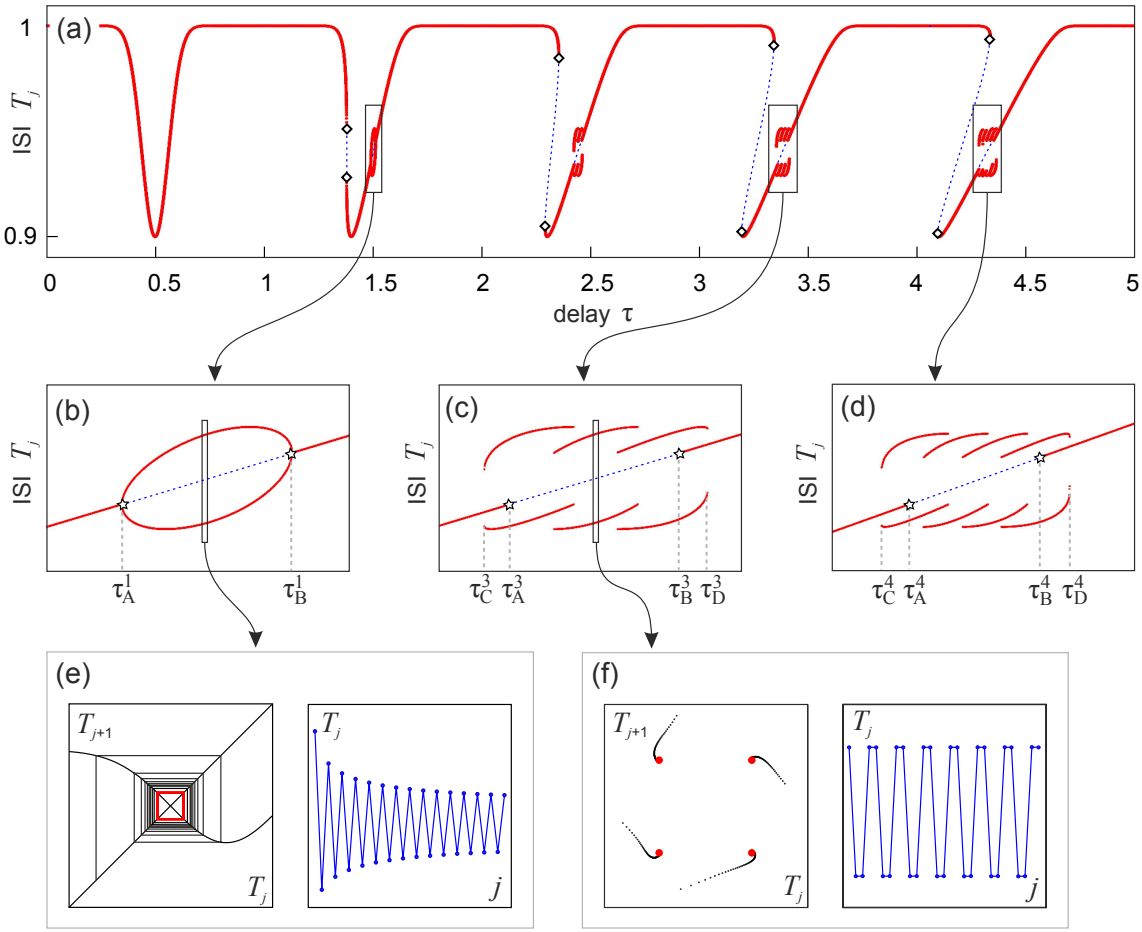

Figure 5: (a) Numerical bifurcation diagram for (1) with PRC (4) where $q = 28$. The delay τ is varied in the range $[0, 5]$. Red dots correspond to ISIs observed in direct simulations; the blue dashed lines corresponds to unstable RS; squares indicate fold bifurcations. (b-d) are zooms into regions of (a) where irregular spiking occurs; stars indicate multi-jitter bifurcations. (e) Left panel: One-dimensional map (16) describing the dynamics of ISIs for $P = 1$ ($\tau = 1.5$), together with a cobweb diagram for a trajectory converging to the stable period-2 solution. Right panel: temporal dynamics, ISIs T_j versus time. (f) Bipartite period-4 solution $(\overline{T_1, T_1, T_2, T_2})$ for $P = 3$ ($\tau = 3.38$). Left panel: a trajectory converging to this solution in the (T_{j+1}, T_j)-plane; Right panel: temporal dynamics.

at $P = 3$ the following period-4 bipartite solutions are observed as τ changes from τ_C^3 to τ_D^3:
(i) $(\overline{T_1, T_1, T_1, T_2})$,
(ii) $(\overline{T_1, T_2}) \equiv (\overline{T_1, T_2, T_1, T_2})$,
(iii) $(\overline{T_1, T_1, T_2, T_2})$,
(iv) $(\overline{T_1, T_2, T_2, T_2})$,
where $T_2 > T_1$. The stability regions of different solutions overlap leading to multistability for the corresponding values of the delay τ. Tripartite solutions of the same period $P + 1$ can be observed in a relatively narrow parameter interval at $P = 2$ [cf. Sec. 5].

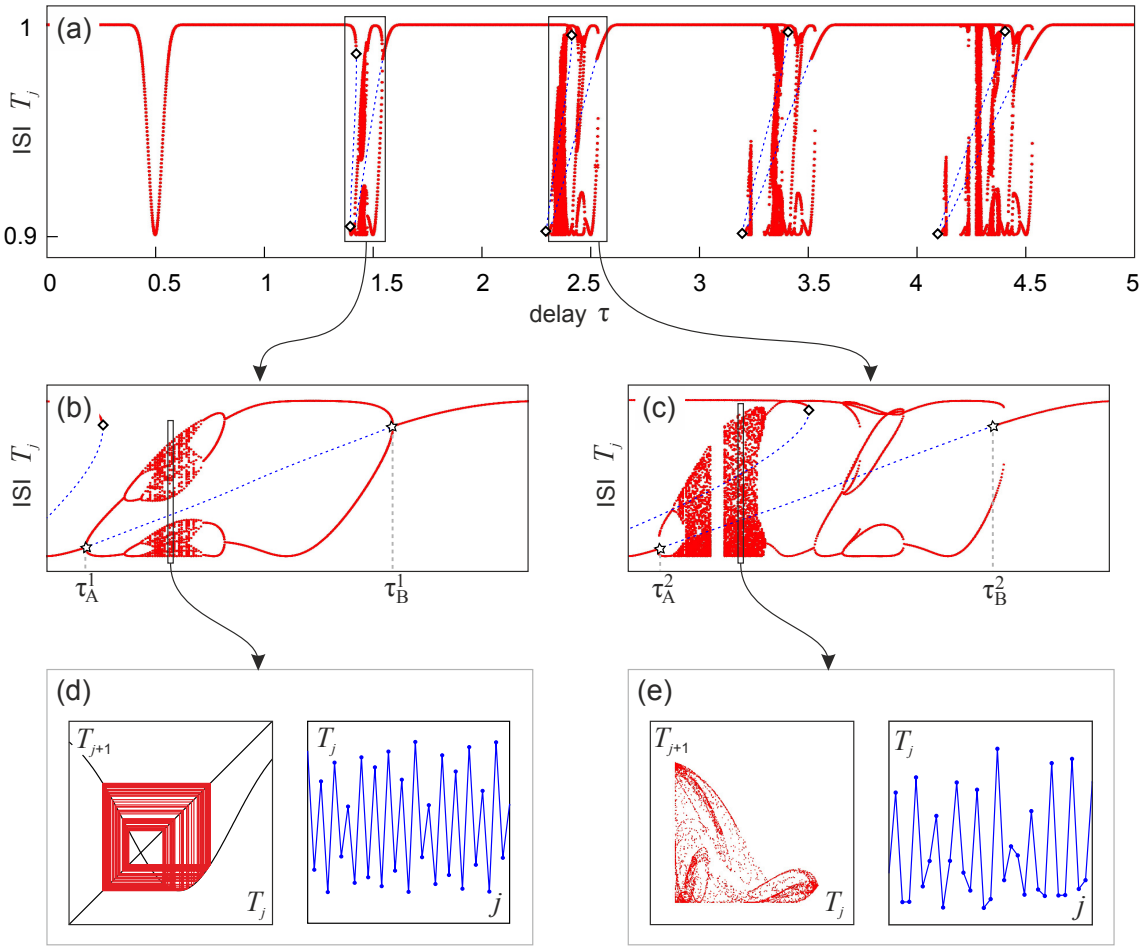

Figure 6: (a) Numerical bifurcation diagram for (1) with PRC (4) where $q = 100$. The delay τ is varied in the range $[0, 5]$. Red dots correspond to ISIs observed in direct simulations; the blue dashed lines correspond to unstable RS; squares indicate fold bifurcations. (b) and (c) are zooms of the indicated regions in (a); stars denote multi-jitter bifurcations. (d) Chaotic solution for $P = 1$ (right) and the corresponding 1-D map (left) for $\tau = 1.445$. (e) Chaotic solution for $\tau = 2.38$ $(P = 2)$ in the (T_j, T_{j+1})-plane (left) and as a temporal sequence (right).

4.3 Large supercritical steepness

Figure 6 shows the case $q = 100$, which is farther beyond the criticality q^* and corresponds to a steepness $s \approx 1.9$. As in the previous case, two points $\tau_{A,B}^P$ exist for each $P = 1, 2, ...$, where $\alpha = -1$, and bifurcations of the RS occur at those points. The instability intervals $[\tau_A^P, \tau_B^P]$ are larger than in Fig. 5 as well as the intervals $\left[\tau_C^P, \tau_D^P\right]$, where jittering regimes appear. Besides the described bi- and tripartite solutions, more complex dynamics is observed inside these intervals. For $P = 1$ the scenario of emergence of this dynamics is similar to that in the one-dimensional logistic map. In this case a cascade of period doubling bifurcations leads to the birth of a chaotic attractor [Fig. 6(b)], which is illustrated in Fig. 6(d). For $P \geq 2$ the observed scenarios include period doubling cascades as well as emergence and destruction of tori which both may lead to the birth of chaotic attractors. An example of such an attractor for the case

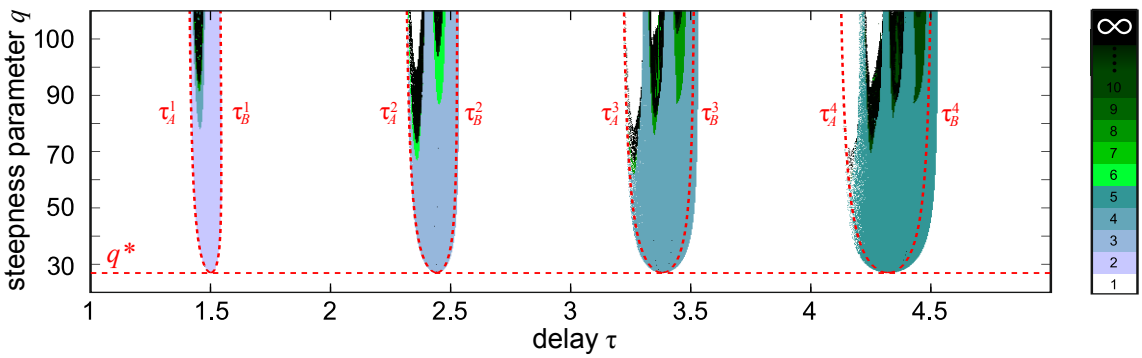

Figure 7: Numerically obtained two-dimensional bifurcation diagram for system (1) with PRC (4). Free parameters are the delay time τ and the steepness parameter q. The maximal observed attractor period is coded in color. White corresponds to period-1 (RS), shades of blue and green correspond to finite numbers larger than one (bipartite and multipartite spiking), black corresponds to quasiperiodic or chaotic spiking, or a period larger than 100. Red solid curves consist of multi-jitter bifurcations points (corresponding to curves $\tau^P_{A,B}(q)$), and dashed red line indicates the critical steepness at $q = q^*$.

$P = 2$ is shown in Fig. 6(e).

A two-dimensional, numerical bifurcation diagram in the parameters τ and q is shown in Fig. 7. The diagram was obtained by simulating (1) with $N = 20$ different random initial values (as for the one-dimensional diagrams in Figs. 5 and 6) for each of 1000×1000 grid points in the shown region $(\tau, q) \in [1, 5] \times [20, 120]$. For each point, the period of the solution is computed after a transient for each of the 20 runs and the maximal observed period was stored to generate the figure. If the period exceeded 100, the observed regime was considered aperiodic (black points).

The largest area (white) in Fig. 7 corresponds to stable RS solutions. For $q > q^*$, islands of irregularity appear, each corresponding to one value of $P = 1, 2, 3....$ The internal structure of these islands is quite complicated. They consist of areas with solutions of different periods, often connected via period doubling bifurcations, as well as areas with quasiperiodic and chaotic solutions. Close to the border of each island there are bipartite period-$(P+1)$ solutions. Deeper in the interior, solutions of higher periods emerge, as well as quasiperiodic and chaotic solutions. However, we also observe windows of regularity inside the irregularity islands.

5 The multi-jitter bifurcation

As it was observed in Secs. 3.2 and 4, a RS solution is destabilized either in a saddle-node bifurcation or in a peculiar bifurcation, where P multipliers become unstable simultaneously. In this section we show that a large number of "jittering" solutions emerges, i.e. solutions with different ISIs, in this "multi-jitter" bifurcation. To prove this we consider the equation

$$1 - T = Z(T - \theta), \tag{17}$$

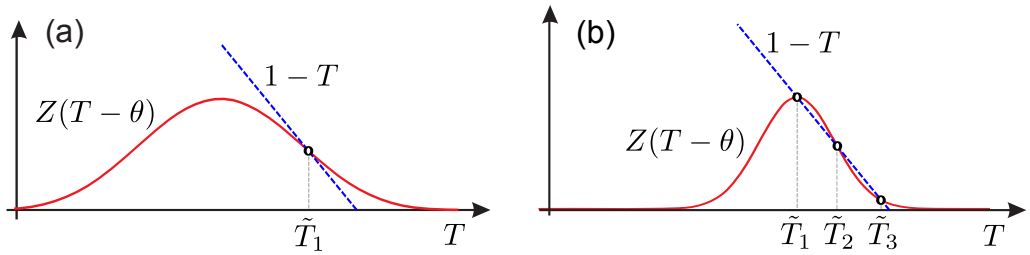

Figure 8: Solutions of Eq. (17) for (a) $s < 1$ and (b) $s > 1$. The solid red line corresponds to the right hand side, the dashed blue line to the left hand side of (17).

where $\theta > 0$ is a constant and $T \in [\theta, \theta + 1]$. As we show below, solutions to this equation can be used as a basis for the construction of periodic solutions of the map (9).

Let us first consider the simplest case, which assumes a single solution $\tilde{T}$ of (17). This implies immediately the existence of RS with period $\tilde{T}$ for the delay values $\tau = \tilde{T} - \theta + P\tilde{T}$, for all $P \in \mathbb{N}$ [cf. Eq. (10)]. This observation of multiple occurrence of the same solution at different values of τ is well known as periodic solution reappearance in delay differential equations [52].

Many more possibilities arise when for some value of θ Eq. (17) has two or more solutions $\tilde{T}_k$. In this case one can construct an arbitrary $(P+1)$-periodic sequence $(\overline{T_1, T_2, ..., T_{P+1}})$ from these values, i.e. $T_j \in \left\{\tilde{T}_k\right\}$, and obtain a periodic solution of the map (9) for

$$\tau = \left(\sum_{j=1}^{P+1} T_j\right) - \theta. \tag{18}$$

This statement is readily confirmed by a direct check. Indeed, for each item T_{j+1} of the sequence $(\overline{T_1, T_2, ..., T_{P+1}})$ we have

$$\begin{aligned} T_{j+1} &= T_{j-P} = 1 - Z(T_{j-P} - \theta) \\ &= 1 - Z\left(\tau - \textstyle\sum_{k=j-P+1}^{j} T_j\right), \end{aligned}$$

which coincides with (9).

Fig. 8 illustrates possible solutions to Eq. (17) for the PRC (4). If the slope of the right hand side, that is of the PRC Z, is not less than -1 for all values of T, only one intersection and only one solution T_1 of (17) exists [Fig. 8(a)]. But if the PRC is steep enough, namely $s > 1$, three different solutions T_1, T_2 and T_3 of (17) exist within a certain interval of θ (Fig. 8(b)). In this case, the values of θ corresponding to the emergence of the new roots can be found from the condition that the left hand and the right hand side of (17) intersect tangentially in θ. These values equal

$$\theta_{A,B} = 1 - \psi_{A,B} - Z(\psi_{A,B}),$$

where $\psi_{A,B}$ are the points where the slope of the PRC equals $Z'(\psi_{A,B}) = -1$. Equation (17) has three different solutions inside the interval $\theta \in [\theta_A, \theta_B]$ and only one solution outside of this interval. It can not have more than three different solutions for the PRC given by (4).

This explains the emergence of bipartite and tripartite solutions which were reported in Sec. 4. They exist for steepness $s > 1$ when Eq. (17) can have more than one solution $\tilde{T}_k$. To construct

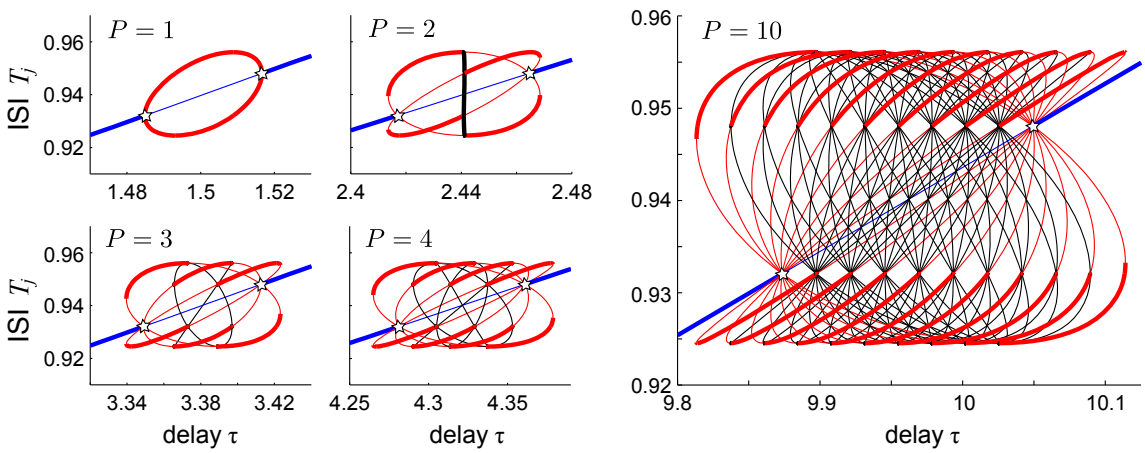

Figure 9: (a)–(d) Branches of RS (blue), bipartite (red), and tripartite (black) solutions in system (1) with PRC (4) and $q = 28$, for different values of P as indicated in the plots. Stable parts of the branches are shown by thick, and unstable by thin lines; stars indicate multi-jitter bifurcations.

all solutions for a given P these solutions $\tilde{T}_k(\theta)$ are determined in dependence of $\theta \in [\theta_A, \theta_B]$ and then composed in all possible periodic sequences of period $\leq P + 1$. A series of the bipartite and tripartite solution branches obtained in this way is shown in Fig. 9 for $q = 28$ and $P = 1, ..., 4$, and $P = 10$. The stability of these solutions was calculated as described in Appendix C.

The obtained stable solutions coincide with the attractors from the bifurcation diagrams in Fig. 5(b)–(d) and complement the diagrams by parts which are difficult to obtain by direct simulation like unstable and tripartite solutions. Each observed bipartite solution corresponds to a pair of points (τ, T_1) and (τ, T_2) on the diagram; each tripartite solution corresponds to three such points. Note that solution branches which contain the same quantities of each contained ISI coincide. For instance, in the case $P = 3$ the branches corresponding to bipartite solutions of the form $(\overline{T_1, T_2}) \equiv (\overline{T_1, T_2, T_1, T_2})$ and $(\overline{T_1, T_1, T_2, T_2})$ lie on top of each other in Fig. 9(c). This increasing number of overlapping branches is the reason for the exponential growth of coexisting solutions and not the number of visibly different branches which equals P. Surprisingly, the stability along the overlapping branches seems to coincide. We formulate this as a conjecture in Appendix C. Notably, there exists only a very narrow interval of τ where stable tripartite solutions exist. These are the solutions $(\overline{T_1, T_2, T_3})$ and $(\overline{T_1, T_3, T_2})$ for $P = 2$. All other tripartite solutions are unstable.

Let us now estimate the number of different bipartite solutions which exist for a given P. Each of this solutions corresponds to a sequence of two ISIs T_1 and T_2 which has the length $P + 1$. For each possibility to write $P + 1 = n_1 + n_2$ with positive integers n_1 and n_2, we obtain $\binom{P+1}{n_1}$ different sequences consisting of n_1 entries equal to T_1 and n_2 entries equal to T_2. Not all of these sequences correspond to different periodic solutions of (9), since some of them might be transformable to others by a periodical shift. Both sequences correspond to the same periodic solution if and only if this is possible. Therefore we can estimate the total number of different $(P + 1)$-periodic solutions containing exactly n_1 ISIs T_1 in their sequential representation to be equal to or larger than $\binom{P+1}{n_1}/(P + 1)$. Here the quotient $(P + 1)$ disregards possible shift

duplicates. Summing up over $n_1 = 1, ..., P$ gives the following estimate for the total number of bipartite solutions existing for P:

$$\#\{\text{bipartite solutions for } P\} \geq \left(2^{P+1} - 2\right)/(P+1). \tag{19}$$

Thus, the number of solutions emerging due to described mechanism grows exponentially with P. Notice that these solutions exist for different intervals of the delay τ. However, all of them emerge in the dimension explosion points $\tau_{A,B}^P$ and exist at least in the interval $[\tau_A^P, \tau_B^P]$.

Indeed, consider a parametrized bipartite solution $(\overline{T_1, ..., T_{P+1}})$ with $T_k = T_k(\theta)$ such that, e.g. $T_k(\theta) \in \{\tilde{T}_1(\theta), \tilde{T}_2(\theta)\}$ [see Fig. 8]. The value of θ, say θ_B, where both basic ISIs $\tilde{T}_1$ and $\tilde{T}_2$ converge to the common value $\tilde{T}_{1,2} \to T = 1 - Z(\psi_B)$ corresponds to the point where the bipartite solution emerges from the branch of RS solutions. At the same time the corresponding delay converges to the value $\tau = P(1 - Z(\psi_B)) + \psi_B = \tau_B^P$. These limits are exactly the values of the ISI and the delay in the points of dimension explosion bifurcation of the RS as obtained from Eq. (15).

This finding is well recognizable by the diagrams in Fig. 9 in which all branches of bipartite solutions start from the dimension explosion points on the RS branch. The full branch of bipartite solutions is obtained as the concatenation of the curves $\theta \mapsto (\tilde{T}_2(\theta), \tilde{T}_3(\theta))$, $\theta \mapsto (\tilde{T}_1(\theta), \tilde{T}_3(\theta))$, and $\theta \mapsto (\tilde{T}_1(\theta), \tilde{T}_2(\theta))$ with θ running back and forth between θ_A and θ_B.

Thus, we have shown that the "dimension explosion" of the unstable manifold, which takes place at the multi-jitter bifurcation of the RS regime is also a "solution explosion". In this bifurcation numerous bipartite solutions branch off, and the number of the emergent solution grows exponentially with the delay τ. Since each of these solutions corresponds to a jittering regime we adopt the term "multi-jitter bifurcation".

6 Experimental observation of bipartite jittering solutions

The multi-jitter bifurcation was discovered and studied in a reduced phase model (1). An important question is whether this bifurcation and the emerging multitude of jittering solutions is a peculiarity of the phase models or it also occurs in realistic setups.

In [32] we have provided some evidence that it also occurs in a realistic neural model and in a physically implemented electronic circuit. We have shown that the regular spiking destabilizes in the points with $Z'(\psi) = -1$ as predicted by our theory and the jittering regimes emerge instead. However, it was not checked whether all of the predicted jittering solutions can be realised. According to (19), their number should increase exponentially with the delay.

We have experimentally studied an electronic FitzHugh-Nagumo oscillator with a long feedback delay [7, 55]. The circuitry of the electronic FitzHugh-Nagumo oscillator as used in the experiment is depicted in Fig. 10(a). Here, $R = 1\text{k}\Omega$, $C = 5\text{nF}$, $L = 9.4\text{H}$, P_{in} is an input from the delay line, and $F(u) = \alpha u(u - u_0)(u + u_0)$ is the current-voltage characteristic of the nonlinear resistor with $\alpha = 2.02 \times 10^{-4}\Omega^{-1}\text{V}^{-2}$ and $u_0 = 0.82\text{V}$. In absence of the delayed feedback, the device exhibits autonomous oscillations with period $T \approx 2.95\text{ms}$. The delay line

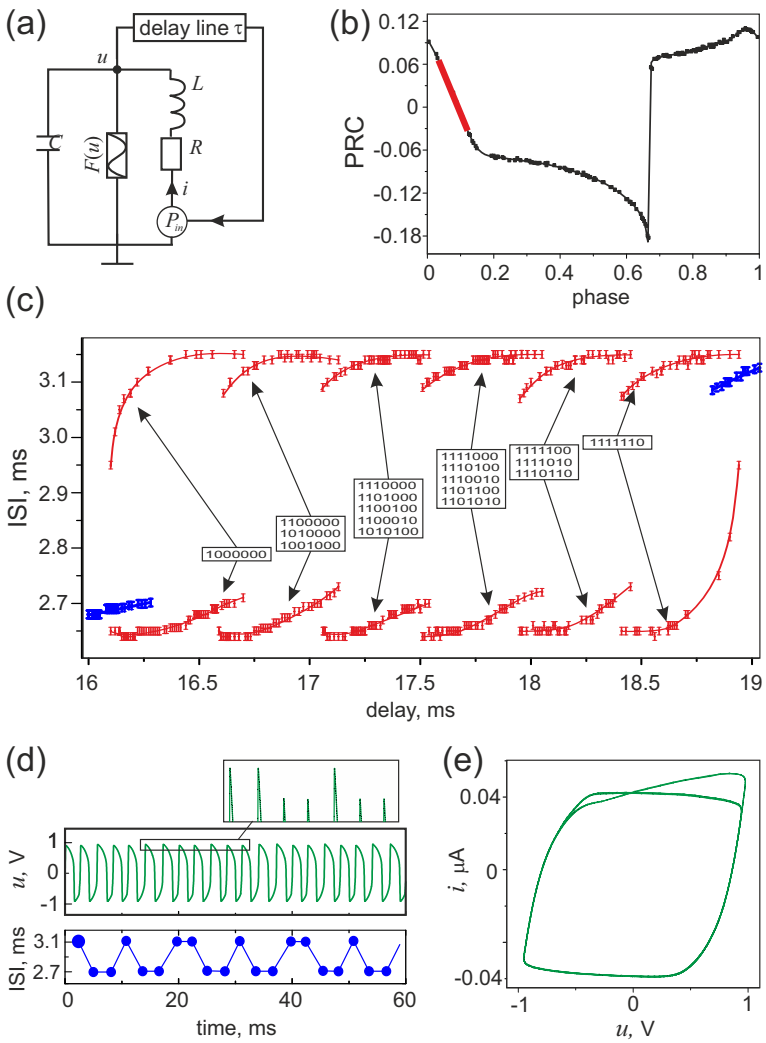

Figure 10: Experimental study of jttering regimes in an oscillatory electronic circuit. (a) Circuitry of the experimental setup. (b) The measured PRC of the electronic oscillator. (c) Bifurcation diagram of the system for $P = 6$: the observed ISIs are plotted against the feedback delay time τ. Blue branches correspond to regular spiking, red to jittering regimes. The binary sequences in the inset boxes correspond to the observed jittering solutions. (d) One of the observed jittering solutions: the dependence of the output voltage u and the ISI on the time. (e) The phase-plane projection of the oscillator in the jittering regime.

is realized on FPGA Xilinx Virtex-5 LX50 and it represents a shift register consisting of 4000 elements with time of the shift less than 7 microseconds. Thus, it provides a delay of a single pulse with an accuracy better than 0.4% of the autonomus oscillation period T. The feedback is delivered as a pulse of amplitude $A = 5$V and duration $\theta = 42\mu$s with a delay τ after each time the voltage u transverses the threshold $u_{th} = -0.7$V in positive direction. For the given parameters, the phase resetting curve of the oscillator has the shape depicted in Fig. 10(b) and exhibits an interval with the slope less than -1 indicated by red color.

During the experiment, we gradually selected different values of the feedback delay time τ, and

recorded the distinct observed dynamical regimes. The results are depicted in the experimental bifurcation diagram in Fig. 10(c). Here, for each delay τ the observed ISIs are plotted analogously to the presentation in Figs. 3–6. One can see that the regular spiking regime with a single value of the ISI is observed for $\tau < \tau_A \approx 16.3$ms and for $\tau > \tau_B \approx 18.8$ms. Inside the interval $[\tau_A; \tau_B]$, the regular spiking regime destabilizes and bipartite jittering solutions are observed. Each bipartite solution corresponds to a pair of points on the bifurcation diagram.

Recall that our theory predicts the coexistence of different bipartite regimes with the same number of short and long ISIs differing only in their order. In the experiment, we have considered values of the delay within the range $\tau \in [16\mathrm{ms}, 19\mathrm{ms}]$ which corresponds to $P = 6$. According to the estimate (19) at least 18 different jittering regimes should exist for the considered values of τ. Each of this regimes can be encoded by a binary sequence of length $P + 1 = 7$ representing a short ISI by zero and a long by one. Not all of these regimes are distinguishable in the bifurcation diagram since some of them are constituted of the same ISIs and thus correspond to the same points. To detect experimentally the coexistence of such solutions we temporarily applied an external noisy signal to induce switches between different attractors. An example of a jittering regime observed is shown in Fig. 10(d). The solution consists of a periodic repetition of four short and three long ISIs. In the phase-plane projection of the system two loops are present corresponding to two ISIs (Fig. 10(e)).

In Fig. 10(c), the observed bipartite regimes along each depicted branch are indicated by the corresponding binary sequences. As predicted by the theory, the branches with the same number of short and long ISIs coincide. Moreover, the delay intervals in which such branches are observed coincide as well. This suggests that, also for the experimental system, the stability of a bipartite regime does only depend on the number of short and long ISIs, not on their order.

7 Discussion

In a phase oscillator with pulsatile feedback (1) the destabilization of the regular spiking mode can occur through a peculiar bifurcation in which the dimension of the unstable manifold "explodes", i.e. changes abruptly from zero to an arbitrary large value. To our opinion, it is remarkable and surprising that the single (and robust) condition $Z'(\varphi) < -1$ induces a destabilization of the regular spiking regime along many directions simultaneously. Normally, bifurcations in which many multipliers become critical simultaneously have large codimension. This means that they take place in low-dimensional subsets of a high-dimensional parameter space. In this sense, the multi-jitter bifurcation in system (1) has codimension one, since it occurs when a scalar equation of the system parameters is fulfilled, namely $Z'(\varphi) = -1$. Varying a single system parameter, e.g. the delay, one can trigger this bifurcation. Thus, it is a degenerate bifurcation which emerges generically. This paradox originates in the structure of the map (9) considered as a $P-$dimensional map

$$\begin{aligned} \boldsymbol{T} &= (T_1, ..., T_P) \\ \mapsto \boldsymbol{T}^{\mathrm{new}} &= (T_1^{\mathrm{new}}, ..., T_P^{\mathrm{new}}) \\ &= (T_2, ..., T_P, 1 - Z(\psi)) \end{aligned} \tag{20}$$

where $\psi = \tau - \sum_{k=1}^{P} T_k$. Besides the calculation of the new ISI $T_P^{\text{new}} = 1 - Z(\psi)$ the map only shifts the past ISIs by one component, which corresponds to the introduction of a comoving timeframe. This results in a specific structure of the map Jacobian

$$D(\alpha) = \begin{bmatrix} 0 & 1 & 0 & 0 \\ \vdots & \ddots & \ddots & 0 \\ 0 & \cdots & 0 & 1 \\ \alpha & \cdots & \cdots & \alpha \end{bmatrix}, \tag{21}$$

where $\alpha = Z'(\psi)$. The matrix $D(\alpha)$ is the companion matrix of the characteristic equation (14). Although one may think of arbitrary perturbations of the map (20) only few of them are physically meaningful. For example, if we introduce an additional parameter ε to alter the first equation of the map such that

$$T_1^{\text{new}} = T_2 + \epsilon g(\boldsymbol{T}),$$

with some function $g : \mathbb{R}^P \to \mathbb{R}$, this would not correspond to a reasonable perturbation because intervals of time do not become longer or shorter while the origin of time is shifted by a comoving timeframe. Similar reasoning reveals that the structure of the whole map should be preserved. It seems that physically admissible perturbations can only affect the delay τ or the PRC shape and all these perturbations exclusively affect the coefficient α in the Jacobian (21) while its structure preserves. Thus, the characteristic equation remains of the form (14) which implies a multi-jitter bifurcation for $\alpha = -1$, where many multipliers become unstable at once.

Besides the discovery of the dimension explosion phenomenon, which is surprising *per se*, we proved that each such bifurcation is accompanied by a potentially huge number of simultaneously emerging jittering solutions. This observation lead us to adopt the name “multi-jitter” bifurcation. More precisely, the number of the emergent coexisting solutions is exponential in the length of the delay τ. This phenomenon is akin to the reappearance of periodic solutions, a well-known property of delay differential equations [52]. Consider a T-periodic solution $x(t) = x(t+T)$ of the general equation

$$\frac{dx}{dt}(t) = f(x(t), x(t-\tau)).$$

Then it is clear from the periodicity of the solution $x(t)$ that it also solves the equation

$$\frac{dx}{dt}(t) = f(x(t), x(t-\tau-PT))$$

for any $P \in \mathbb{N}$. It means, that the same periodic solution reappears at the delay times $\tau_P = \tau + PT$. Note that the stability of the reappearing solution can be different for different delay times (see more details in [56]). The number of coexisting reappearant solutions increases linearly with the delay time, which can be accessed intuitively from the observation that the reappearing branch of solutions is stretched proportionally to the reappearance index P and the change in period along the branch [cf. the branch of RS solutions in Fig. 3].

In contrast to this type of reappearance, the reappearant solutions in system (1) may not be identical to the original solution, but the possibility of ISI reordering allows for the emergence

of a multitude of new solutions. Thus, we observe reappearance not of whole solutions, but of individual ISIs, which leads us to propose to call the phenomenon "quasi-reappearance". For instance, the existence of a period-2 solution with the ISIs T_1 and T_2 implies the existence of infinitely many bipartite solutions which exhibit exactly these ISIs for larger delays. In fact, *every* periodical sequence of these two ISIs will correspond to a solution of (1) for an appropriate value of the delay. Indeed, if the sequence $(\overline{T_1, T_2})$ solves (9) for some $\tau = \tau_0$, and arbitrary periodical sequence of the two ISIs containing n_1 instances of T_1 and n_2 instances of T_2 per period solves (9) for

$$\tau = \tau_0 + (n_1 - 1)\, T_1 + (n_2 - 1)\, T_2. \tag{22}$$

The combinatorial variety of the quasi-reappearant solutions causes an exponential increase of their number with the delay. Therefore the multistability of the system increases potentially much faster than due to ordinary reappearance.

An interesting property following from this mechanism of quasi-reappearance is that the τ-intervals for the existence of the jittering regimes at a certain P are ordered according to the corresponding number of short/long ISIs [see, e.g., Fig. 10(c)]. The regime with just *one* long ISI is stable for the smallest values of τ in the region corresponding to P. Subsequently, the three regimes with *two* long ISIs stabilize for larger τ, then the regimes with *three* long ISIs stabilize and so on. It is also noteworthy that the intervals of stability of the regimes with n_1 and $n_1 + 1$ long ISIs may overlap giving rise to even greater multistability. This feature is also confirmed by the experiment: for example, for $\tau = 17.52$ms, ten different jittering regimes are observed [cf. Fig. 10(c)].

We would also like to comment on the relevance of the multi-jittering phenomenon to more realistic setups, where the oscillator's phase space has a higher dimension than one and the pulse is smooth and of finite duration. We have demonstrated that the multi-jitter instability can appear in real electronic circuit as well as in a simulated Hodgkin-Huxley neuron model [32] and it might be one of the mechanisms behind the appearance of irregular spiking in neuronal models with delayed feedback [43] and timing jitter in semiconductor laser systems with delayed feedback [10] reported by other authors.

Our theory predicts and our numerical simulations confirm that the essential property for the occurrence of a dimension explosion bifurcation is the steepness of the PRC corresponding to the pulsatile feedback action. The presence of regions where the slope of the PRC fulfills $Z'(\varphi) < -1$ requires some specific organization of the oscillator's phase space. Consider the phase transition map

$$f(\varphi) = \varphi + Z(\varphi), \tag{23}$$

which describes change of the oscillator's phase under the action of the feedback pulse. Notice that $Z'(\varphi) < -1$ for some φ if and only if the phase transition map is non-monotonous. This means that the input can inverse the phase order of some points from the limit cycle, such that $f(\varphi_2) < f(\varphi_1)$ for some $\varphi_2 > \varphi_1$.

This feature can be interpreted geometrically as a property of the isochrons in the oscillator's phase space. The isochrons are sets consisting of points that have the same phase, i.e., their distance vanishes for $t \to \infty$ as they are attracted to the limit cycle [3, 57–59]. The new phase

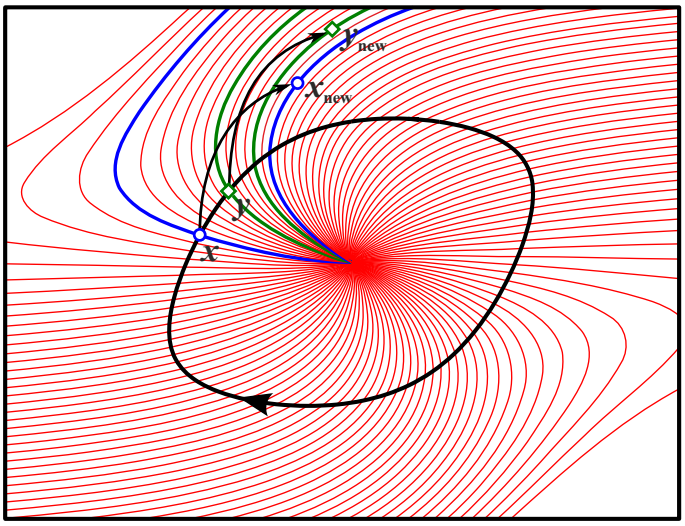

Figure 11: The isochrons of a FitzHugh-Nagumo model show the structure necessary for $Z'(\varphi) < -1$. The phase order of two different points on the limit cycle, x and y, is reversed by the corresponding pulse. This means they are carried to new points x_{new} and y_{new} which lie on isochrons with a reversed phase order.

$\varphi_{\text{new}} = f(\varphi)$ induced by a pulse, which starts when the oscillator is located at phase φ on the limit cycle, is determined by the isochron to which the point with the phase φ is conveyed by the pulse. The fact that the input inverses the phase order of some neighboring points from the limit cycle implies that the point of smaller phase transverses more isochrons than the other. If the direction of the pulse does not change, which typically leads to a straight displacement of the oscillator's state [60, 61], the isochrons should have a specific form of nested u-shaped curves. This is illustrated in Fig. 11 for the FitzHugh-Nagumo system.

Thus, the discovered dimension explosion and multi-jittering phenomena are relevant not only for a simple phase-reduced model, but for realistic oscillatory systems as well. A promising application for systems exhibiting high-dimensional complex dynamics is their utilization as liquid state machines. For lasers with long delayed feedback this has been done successfully [62]. In view of the arbitrarily high dimensional critical manifolds of the RS solution, which were observed in this paper, it seems to be worth studying such computational abilities for an oscillator with delayed pulsatile feedback. An electronic implementation of such systems is relatively uncomplicated [7, 32, 55].

8 Conclusions

In this paper we have studied the dynamics of oscillators with pulsatile delayed self-feedback where we directed our attention to the influence and interplay of the feedback delay and the shape of the oscillator's PRC. As a major result we have proven that, if the oscillator's PRC possesses sufficiently steep parts, the system undergoes a sequence of degenerate bifurcations as the feedback delay is increased. These multi-jitter bifurcations lead to a destabilization of

the regular spiking regime through the emergence of an unstable manifold of arbitrarily large dimension, which is proportional to the delay size.

Moreover, we proved that each multi-jitter bifurcation is accompanied by emergence of numerous “jittering” periodic solutions with distinct ISIs. We showed that the mechanism of emergence of such solutions generalizes what is known as reappearance of periodic solutions. In this “quasi-reappearance”, individual ISIs of solutions existing for smaller values of the delay reappear. Thus, when the delay is increased the number of different solutions grows combinatorially causing high multistability and extremely complex structure of the system’s phase space.

Appendix

A Steepness of (4)

Here we estimate the steepness [cf. (5)] of the function $Z(\varphi) = \kappa \left(\sin\left(\pi\varphi\right)\right)^q$ for $\kappa > 0$ and $q \gg 1$. The slope equals

$$Z'(\varphi) = \kappa\pi q \left(\sin\left(\pi\varphi\right)\right)^{q-1} \cos\left(\pi\varphi\right).$$

It is extremal for $\varphi^* \in (0,1)$ with

$$\begin{aligned}
&Z''(\varphi^*)\\
=&\kappa\pi^2 q(q-1)\left(\sin\left(\pi\varphi^*\right)\right)^{q-2}\left(\cos\left(\pi\varphi^*\right)\right)^2\\
&-\kappa\pi^2 q\left(\sin\left(\pi\varphi^*\right)\right)^q\\
=&\kappa\pi^2 q\left(\sin\left(\pi\varphi^*\right)\right)^{q-2}\left(q\left(\cos\left(\pi\varphi^*\right)\right)^2-1\right)=0
\end{aligned}$$

In this point, we have

$$\cos\left(\pi\varphi^*\right) = \pm\sqrt{\frac{1}{q}}, \text{ and } \sin\left(\pi\varphi^*\right) = \pm\sqrt{1-\frac{1}{q}} \approx \pm(1-\frac{1}{2q}).$$

Hence, the steepness can be calculated as

$$\begin{aligned}
s = |Z'(\varphi^*)| &= |\kappa\pi q \left(\sin\left(\pi\varphi^*\right)\right)^{q-1}\cos\left(\pi\varphi^*\right)|\\
&\approx \kappa\pi q\left(1-\frac{1}{2q}\right)^{q-1}\frac{1}{\sqrt{q}} \approx \kappa\pi\sqrt{\frac{q}{e}},
\end{aligned}$$

where e is Euler's number.

B RS Spectrum

Here we study the roots of the characteristic equation (14). For convenience, we restate the properties of the spectrum asserted in Section 3.2:

(A) For $-1 < \alpha < 1/P$, all multipliers λ_k, $k = 1, ..., P$, have absolute value less than one.

(B) At $\alpha = 1/P$ a critical multiplier crosses the unit circle at $\lambda = 1$. For $\alpha > 1/P$ this multiplier remains unstable.

(C) At $\alpha = -1$ there are P critical multipliers $\lambda_k = e^{i2\pi k/(P+1)}$, $k = 1, \ldots, P$, crossing $|\lambda| = 1$ simultaneously. For $\alpha < -1$, there are P unstable multipliers with $|\lambda_k| > 1$, $k = 1, \ldots, P$.

To prove these claims, we multiply the characteristic polynomial $\chi_{P,\alpha}(\lambda)$ by $(\lambda - 1)$ and study the extended characteristic equation

$$\begin{aligned}
\tilde{\chi}_{P,\alpha}(\lambda) &= (\lambda-1)\,\chi_{P,\alpha}(\lambda)\\
&= \lambda^{P+1} - (1+\alpha)\lambda^P + \alpha = 0.
\end{aligned} \tag{24}$$

The set $\tilde{\Lambda}$ of roots of $\tilde{\chi}_{P,\alpha}(\lambda)$ contains all roots $\Lambda = \{\lambda_1, ..., \lambda_P\}$ of $\chi_{P,\alpha}(\lambda)$ and the root $\lambda_{P+1} = 1$, i.e., $\Lambda = \tilde{\Lambda}\backslash\{1\}$ for $\alpha \neq 1/P$. In the following, we study the critical roots of $\tilde{\chi}_{P,\alpha}(\lambda)$, i.e. solutions of (24) with $|\lambda| = 1$. Substituting $\lambda = e^{i\varphi}$ into (24) we obtain

$$e^{i(P+1)\varphi} + \alpha = (1+\alpha)e^{iP\varphi}. \tag{25}$$

Taking the absolute value on both sides of (25) yields

$$\left|e^{i(P+1)\varphi} + \alpha\right| = |1+\alpha|,$$

which, for $\alpha \neq 0$, implies $e^{i(P+1)\varphi} = 1$. This means $\varphi = 2\pi k/(P+1)$ for some $k \in \mathbb{Z}$. Substituting this into (25) gives

$$1 + \alpha = (1+\alpha)e^{i2\pi kP/(P+1)}.$$

For $\alpha \neq -1$, this requires $k \in (P+1)\mathbb{Z}$. Thus, for $\alpha \notin \{-1, 0\}$, $\lambda = 1$ is the only solution of (24) with $|\lambda| = 1$. It corresponds to a critical multiplier of (14) only for $\alpha = 1/P$, where it is a double root of (24). Indeed, substituting $\lambda = 1$ into (14) one obtains $1 - P\alpha = 0$. For $\alpha = -1$, (24) reduces to

$$\lambda^{P+1} = 1.$$

Hence, P critical multipliers $\lambda_k = e^{i2\pi k/(P+1)}$, $k = 1, ..., P$, appear simultaneously at $\alpha = -1$. For $\alpha = 0$, (14) reduces to $\lambda^P = 0$, which obviously exhibits no critical multipliers.

Finally let us remark that, with respect to α, all critical roots $\lambda(\alpha)$ of $\chi_{P,\alpha}$ traverse the unit cycle at criticality $|\lambda(\alpha)| = 1$ and for $\alpha = 0$ all multipliers vanish identically: $\lambda_1(0) = ... = \lambda_P(0) = 0$. This completes the prove of (A)–(C).

For $P \gg 1$ a deeper study of the multipliers of (14) is possible. One may follow the concept developed in [63] and determine the so-called "strong" and "weak" multipliers. Strong multipliers λ_s are characterized by the fact that $\lim_{P\to\infty} \lambda_s(P) = \lambda_s$. The only strong multiplier of (14) equals $\lambda_s \approx 1 + \alpha$ for large P, which means that the strong spectrum is unstable for $\alpha > 0$ and $\alpha < -2$. Weak multipliers λ_w are characterized by the following asymptotic behavior for large P: $\lambda_w(P) \approx e^{\mu/P + i\omega}$. The weak multipliers of (14) are given by the relationship

$$\mu = -\frac{1}{2}\ln\left(1 + \frac{(1+\alpha)(1-\cos\omega)}{\alpha^2}\right). \tag{26}$$

The equation (26) defines a curve on the complex plane on which the weak multipliers reside. For $\alpha > -1$ the curve resides within the unity circle, which means that the weak spectrum is stable. For $\alpha < -1$ the curve lies outside of the unity circle, and the complete weak spectrum becomes unstable at once.

C Stability of multipartite solutions

A multipartite solution is a $P+1$-periodic solution $(\overline{T_1^*, ..., T_{P+1}^*})$ of the ISI map (9). Equivalently, it corresponds to a $P+1$-periodic point $\boldsymbol{T}^* = (T_2^*, ..., T_{P+1}^*)$ of the P-dimensional return map

$\boldsymbol{T} \mapsto \boldsymbol{T}^{\text{new}} = R(\boldsymbol{T})$ given by (20). As such we study its stability, which can be determined from the spectrum of the Jacobian of R^{P+1}

$$\begin{aligned}\mathcal{J} &= D_{\boldsymbol{T}}\left[R^{P+1}\right](\boldsymbol{T}^*) \\ &= D_{\boldsymbol{T}}R(R^P(\boldsymbol{T}^*)) \cdot D_{\boldsymbol{T}}R(R^{P-1}(\boldsymbol{T}^*)) \cdots D_{\boldsymbol{T}}R(\boldsymbol{T}^*).\end{aligned} \tag{27}$$

Since the nonlinear part of $R(\boldsymbol{T})$ depends exclusively on the sum $\sum T_k$, its Jacobian does so equally, i.e.,

$$D_{\boldsymbol{T}}R(\boldsymbol{T}) = D(\alpha),$$

where $\alpha = Z'(\tau - \sum T_k)$ and $D(\alpha)$ is given by Eq. (21). For a $P+1$-periodic point $\boldsymbol{T}^*$, one application of the return map yields

$$R(\boldsymbol{T}^*) = (T_3^*, ..., T_{P+1}^*, T_1^*),$$

and in general, after k applications, we obtain

$$R^k(\boldsymbol{T}^*) = (T_{[1+k]+1}^*, ..., T_{[P+k]+1}^*),$$

with $[n] := n \bmod (P+1)$. Therefore, the factor $D_{\boldsymbol{T}}R(R^k(\boldsymbol{T}^*))$, $k = 0, ..., P$, of $\mathcal{J}$ is given by (21) with

$$\alpha = \alpha_{k+1} = 4Z'\left(\tau - \sum_{j=1}^{P+1} T_j^* + T_{k+1}^*\right). \tag{28}$$

The matrix $\mathcal{J}$ is therefore given as

$$\mathcal{J} = D(\alpha_{P+1}) \cdot D(\alpha_P) \cdots D(\alpha_1). \tag{29}$$

Its spectrum can be obtained numerically. Due to (28), for $T_j^* = T_k^*$, we have $\alpha_j = \alpha_k$. Although we lack a proof, it seems that the spectrum of (29) does not depend on the order of the factors $D(\alpha_k)$, such that the stability of solutions on all overlapping branches in Fig. 9 coincides. More precisely, we conjecture that the characteristic polynomial of (29) has the form

$$\begin{aligned}\det(\mathcal{J} - \lambda) =& \lambda^P - (s_2 + ... + s_{P+1})\lambda^{P-1} - ... \\ & ... - (s_P + s_{P+1})\lambda^1 - s_{P+1},\end{aligned}$$

where $s_j = s_j(\alpha_1, ..., \alpha_{P+1})$ is the j-th symmetric function. For instance, $s_1 = \sum_{k=1}^{P+1} \alpha_k$, $s_2 = \sum_{k=1, j>k}^{P+1} \alpha_k \alpha_j$, and $s_{P+1} = \prod_{k=1}^{P+1} \alpha_k$.

References

[1] A. M. Kunysz, A. Shrier, and L. Glass. Bursting behavior during fixed-delay stimulation of spontaneously beating chick heart cell aggregates. *American Journal of Physiology - Cell Physiology*, 273(1):C331–C346, 1997.

[2] R. Mirollo and S. Strogatz. Synchronization of pulse-coupled biological oscillators. *SIAM J. Appl. Math.*, 50(6):1645–1662, 1990.

[3] A.T. Winfree. *The geometry of biological time*. Springer, 2001.

[4] P. Brzeski, T. Kapitaniak, and P. Perlikowski. Experimental verification of the hybrid dynamical model of the church bell. *International Journal of Impact Engineering*, (0):–, 2015.

[5] Abel Lopera, Javier M. Buldú, M. C. Torrent, Dante R. Chialvo, and Jordi García-Ojalvo. Ghost stochastic resonance with distributed inputs in pulse-coupled electronic neurons. *Phys. Rev. E*, 73:021101, Feb 2006.

[6] David P. Rosin, Damien Rontani, Daniel J. Gauthier, and Eckehard Schöll. Control of synchronization patterns in neural-like boolean networks. *Phys. Rev. Lett.*, 110:104102, Mar 2013.

[7] Vladimir V. Klinshov, Dmitry S. Shchapin, and Vladimir I. Nekorkin. Cross-frequency synchronization of oscillators with time-delayed coupling. *Phys. Rev. E*, 90:042923, Oct 2014.

[8] Pere Colet and Rajarshi Roy. Digital communication with synchronized chaotic lasers. *Opt. Lett.*, 19(24):2056–2058, 1994.

[9] Robert W. Boyd and Daniel J. Gauthier. Controlling the velocity of light pulses. *Science*, 326(5956):1074–1077, 2009.

[10] C Otto, K Lüdge, A G Vladimirov, M Wolfrum, and E Schöll. Delay-induced dynamics and jitter reduction of passively mode-locked semiconductor lasers subject to optical feedback. *New Journal of Physics*, 14(11):113033, 2012.

[11] D C Michaels, E P Matyas, and J Jalife. A mathematical model of the effects of acetylcholine pulses on sinoatrial pacemaker activity. *Circulation Research*, 55(1):89–101, 1984.

[12] S Dokos, BG Celler, and NH Lovell. Vagal control of sinoatrial rhythm: A mathematical model. *JOURNAL OF THEORETICAL BIOLOGY*, 182(1):21–44, SEP 7 1996.

[13] D. G. Tsalikakis, D. I. Fotiadis, L. K. Michalis, and G. P. Kremmydas. Phase resetting in one-dimensional model of the sinoatrial node. *IEEE TRANSACTIONS ON BIOMEDICAL ENGINEERING*, 54(9):1710–1714, SEP 2007.

[14] John Lewis, Manjit Bachoo, Leon Glass, and Canio Polosa. Complex dynamics resulting from repeated stimulation of nonlinear oscillators at a fixed phase. *Physics Letters A*, 125(2-3):119 – 122, 1987.

[15] John E. Lewis, Leon Glass, Manjit Bachoo, and Canio Polosa. Phase resetting and fixed-delay stimulation of a simple model of respiratory rhythm generation. *Journal of Theoretical Biology*, 159(4):491 – 506, 1992.

[16] David S. Minors, James M. Waterhouse, and Anna Wirz-Justice. A human phase-response curve to light. *Neuroscience Letters*, 133(1):36 – 40, 1991.

[17] L. F. Abbott and Carl van Vreeswijk. Asynchronous states in networks of pulse-coupled oscillators. *Phys. Rev. E*, 48(2):1483–1490, Aug 1993.

[18] M. Tsodyks, I. Mitkov, and H. Sompolinsky. Pattern of synchrony in inhomogeneous networks of oscillators with pulse interactions. *Phys. Rev. Lett.*, 71(8):1280–1283, Aug 1993.

[19] U. Ernst, K. Pawelzik, and T. Geisel. Synchronization induced by temporal delays in pulse-coupled oscillators. *Phys. Rev. Lett.*, 74(9):1570–1573, Feb 1995.

[20] S. Bottani. Pulse-coupled relaxation oscillators: From biological synchronization to self-organized criticality. *Phys. Rev. Lett.*, 74:4189–4192, May 1995.

[21] C. van Vreeswijk. Partial synchronization in populations of pulse-coupled oscillators. *Phys. Rev. E*, 54(5):5522–5537, Nov 1996.

[22] P. C. Bressloff, S. Coombes, and B. de Souza. Dynamics of a ring of pulse-coupled oscillators: Group-theoretic approach. *Phys. Rev. Lett.*, 79(15):2791–2794, 1997.

[23] U. Ernst, K. Pawelzik, and T. Geisel. Delay-induced multistable synchronization of biological oscillators. *Physical Review E*, 57(2):2150–2162, February 1998.

[24] P. Goel and B. Ermentrout. Synchrony, stability, and firing patterns in pulse-coupled oscillators. *Physica D: Nonlinear Phenomena*, 163(3-4):191 – 216, 2002.

[25] Enrico Rossoni, Yonghong Chen, Mingzhou Ding, and Jianfeng Feng. Stability of synchronous oscillations in a system of hodgkin-huxley neurons with delayed diffusive and pulsed coupling. 71, 2005.

[26] R. Zillmer, R. Livi, A. Politi, and A. Torcini. Stability of the splay state in pulse-coupled networks. *Phys. Rev. E*, 76(4):046102, 2007.

[27] S. Achuthan and C. Canavier. Phase-resetting curves determine synchronization, phase locking, and clustering in networks of neural oscillators. *The Journal of Neuroscience*, 29(16):5218–5233, 2009.

[28] C.C. Canavier and S. Achuthan. Pulse coupled oscillators and the phase resetting curve. *Mathematical biosciences*, 226(2):77–96, 2010.

[29] M. Drew LaMar and Gregory D. Smith. Effect of node-degree correlation on synchronization of identical pulse-coupled oscillators. *Phys. Rev. E*, 81(4):046206, Apr 2010.

[30] Leonhard Lücken and Serhiy Yanchuk. Two-cluster bifurcations in systems of globally pulse-coupled oscillators. *Physica D: Nonlinear Phenomena*, 241:350–359, 2012.

[31] Leonhard Lücken, Serhiy Yanchuk, Oleksandr V. Popovych, and Peter A. Tass. Desynchronization boost by non-uniform coordinated reset stimulation in ensembles of pulse-coupled neurons. *Frontiers in Computational Neuroscience*, 7:63, 2013.

[32] Vladimir Klinshov, Leonhard Lücken, Dmitry Shchapin, Vladimir Nekorkin, and Serhiy Yanchuk. Multistable jittering in oscillators with pulsatile delayed feedback. *Phys. Rev. Lett.*, 114:178103, 2015.

[33] Eugene M. Izhikevich. *Dynamical Systems in Neuroscience: The Geometry of Excitability and Bursting*. The MIT Press, 2005.

[34] Y. Kuramoto. *Chemical Oscillations, Waves, and Turbulence*. Springer, Berlin, 1984.

[35] Bard Ermentrout. Type i membranes, phase resetting curves, and synchrony. *Neural Computation*, 8(5):979–1001, 1996.

[36] Peter Tass. *Phase Resetting in Medicine and Biology. Stochastic Modelling and Data Analysis*. Springer Series in Synergetics. Springer, 1999.

[37] Viktor Novicenko and Kestutis Pyragas. Computation of phase response curves via a direct method adapted to infinitesimal perturbations. *Nonlinear Dynamics*, pages 1–10, 2011. 10.1007/s11071-011-0001-y.

[38] Leon Glass, Michael R. Guevara, Jacques Belair, and Alvin Shrier. Global bifurcations of a periodically forced biological oscillator. *Phys. Rev. A*, 29:1348–1357, Mar 1984.

[39] J M Anumonwo, M Delmar, A Vinet, D C Michaels, and J Jalife. Phase resetting and entrainment of pacemaker activity in single sinus nodal cells. *Circulation Research*, 68(4):1138–53, 1991.

[40] Roberto F. Galán, G. Bard Ermentrout, and Nathaniel N. Urban. Efficient estimation of phase-resetting curves in real neurons and its significance for neural-network modeling. *Phys. Rev. Lett.*, 94:158101, Apr 2005.

[41] G.Bard Ermentrout, II Beverlin, Bryce, Todd Troyer, and TheodenI. Netoff. The variance of phase-resetting curves. *Journal of Computational Neuroscience*, 31(2):185–197, 2011.

[42] R. Milo, S. Shen-Orr, S. Itzkovitz, N. Kashtan, D. Chklovskii, and U. Alon. Network motifs: Simple building blocks of complex networks. *Science*, 298(5594):824–827, 2002.

[43] Jianfu Ma and Jianhong Wu. Multistability in spiking neuron models of delayed recurrent inhibitory loops. *Neural computation*, 19(8):2124–2148, 2007.

[44] J. Ma and J. Wu. Patterns, memory and periodicity in two-neuron delayed recurrent inhibitory loops. *Mathematical Modelling of Natural Phenomena*, 5:67–99, 1 2010.

[45] M. Hashemi, A. Valizadeh, and Y. Azizi. Effect of duration of synaptic activity on spike rate of a hodgkin-huxley neuron with delayed feedback. *Phys. Rev. E*, 85:021917, Feb 2012.

[46] Guy Van der Sande, Miguel C. Soriano, Ingo Fischer, and Claudio R. Mirasso. Dynamics, correlation scaling, and synchronization behavior in rings of delay-coupled oscillators. *Phys. Rev. E*, 77:055202, 2008.

[47] M. Kantner and S. Yanchuk. Bifurcation analysis of delay-induced patterns in a ring of Hodgkin-Huxley neurons. *Phil. Trans. Roy. Soc. A*, 371:20120470, 2013.

[48] S. Yanchuk, P. Perlikowski, O. V. Popovych, and P. A. Tass. Variability of spatio-temporal patterns in non-homogeneous rings of spiking neurons. *Chaos*, 21:047511, 2011.

[49] V. Flunkert, S. Yanchuk, T. Dahms, and E. Schöll. Synchronizing distant nodes: A universal classification of networks. *Phys. Rev. Lett.*, 105(25):254101, 2010.

[50] Jennifer Foss, André Longtin, Boualem Mensour, and John Milton. Multistability and delayed recurrent loops. *Phys. Rev. Lett.*, 76:708–711, 1996.

[51] Jennifer Foss and John Milton. Multistability in recurrent neural loops arising from delay. *J Neurophysiol*, 84:975–985, 2000.

[52] S. Yanchuk and P. Perlikowski. Delay and periodicity. *Phys. Rev. E*, 79(4):046221, 2009.

[53] B. Ermentrout and N. Kopell. Multiple pulse interactions and averaging in systems of coupled neural oscillators. *J. Math. Biol.*, 29:195–217, 1991.

[54] VV Klinshov and VI Nekorkin. The map with no predetermined firing order for the network of oscillators with time-delayed pulsatile coupling. *Communications in Nonlinear Science and Numerical Simulation*, 18(4):973–977, 2013.

[55] D.S. Shchapin. Dynamics of two neuronlike elements with inhibitory feedback. *Journal of Communications Technology and Electronics*, 54(2):175–184, 2009.

[56] J. Sieber, M. Wolfrum, M. Lichtner, and S. Yanchuk. On the stability of periodic orbits in delay equations with large delay. *Discrete Contin. Dyn. Syst. A*, 33:3109–3134, 2013.

[57] J. Guckenheimer. Isochrons and phaseless sets. *Journal of Mathematical Biology*, 1:259–273, 1975.

[58] Langfield, Peter, Krauskopf, Bernd, and Osinga Hinke M.. Solving Winfree's puzzle: the isochrons in the FitzHugh-Nagumo model, *Chaos*, 24:013131, 2014.

[59] Osinga Hinke M. and Moehlis, Jeff, Continuation-based Computation of Global Isochrons. *SIAM J. Applied Dynamical Systems*, 9:1201–1228, 2010.

[60] V. B. Kazantsev, V. I. Nekorkin, V. I. Makarenko, and R. Llinás Self-referential phase reset based on inferior olive oscillator dynamics. *Proc. Nat. Acad. Sci.*, 101(52):18183–18188, 2004.

[61] V. V. Klinshov, V. I. Nekorkin. Phase reset of complex oscillations by a pulsed action. *JETP Letters*, 87(2):78–82, 2008.

[62] L. Appeltant, M. C. Soriano, G. Van der Sande, J. Danckaert, S. Massar, J. Dambre, B. Schrauwen, C. R. Mirasso, and I. Fischer. Information processing using a single dynamical node as complex system. *Nature Comm*, 2, 2011.

[63] Sven Heiligenthal, Thomas Dahms, Serhiy Yanchuk, Thomas Jüngling, Valentin Flunkert, Ido Kanter, Eckehard Schöll, and Wolfgang Kinzel. Strong and weak chaos in nonlinear networks with time-delayed couplings. *Phys. Rev. Lett.*, 107:234102, 2011.